Mechanism of Scaffolding-Directed Virus Assembly Suggested by Comparison of Scaffolding-Containing and Scaffolding-Lacking P22 Procapsids

Pamela A. Thuman-Commike,* Barrie Greene,# Justine A. Malinski,* Michelle Burbea,§ Amy McGough,* Wah Chiu,* and Peter E. Prevelige, Jr.§

*Department of Biochemistry, Baylor College of Medicine, Houston, Texas 77030; #G. W. Hooper Foundation, University of California San Francisco, San Francisco, California 94143; and §Department of Microbiology, University of Alabama at Birmingham, Birmingham, Alabama 35294, USA

ABSTRACT Assembly of certain classes of bacterial and animal viruses requires the transient presence of molecules known as scaffolding proteins, which are essential for the assembly of the precursor procapsid. To assemble a procapsid of the proper size, each viral coat subunit must adopt the correct quasiequivalent conformation from several possible choices, depending upon the *T* number of the capsid. In the absence of scaffolding protein, the viral coat proteins form aberrantly shaped and incorrectly sized capsids that cannot package DNA. Although scaffolding proteins do not form icosahedral cores within procapsids, an icosahedrally ordered coat/scaffolding interaction could explain how scaffolding can cause conformational differences between coat subunits. To identify the interaction sites of scaffolding protein with the bacteriophage P22 coat protein lattice, we have determined electron cryomicroscopy structures of scaffolding-containing and scaffolding-lacking procapsids. The resulting difference maps suggest specific interactions of scaffolding protein with only four of the seven quasiequivalent coat protein conformations in the $T = 7$ P22 procapsid lattice, supporting the idea that the conformational switching of a coat subunit is regulated by the type of interactions it undergoes with the scaffolding protein. Based on these results, we propose a model for P22 procapsid assembly that involves alternating steps in which first coat, then scaffolding subunits form self-interactions that promote the addition of the other protein. Together, the coat and scaffolding provide overlapping sets of binding interactions that drive the formation of the procapsid.

INTRODUCTION

Regulated protein self-assembly directs the formation of many essential biological structures, from the filaments of the cytoskeleton and extracellular matrix, to vesicle coats, bacterial flagella, and viral capsids. A critical level of control is often provided by various accessory proteins, which determine the timing, site, and extent of assembly, as well as features of the completed structure. In the case of helical microtubules and actin filaments, binding proteins control initiation, extension, and shortening of filaments and may even alter filament structure (Hirokawa, 1994; Mandelkow and Mandelkow, 1995; McGough, 1998). The assembly of clathrin protein subunits into spherical cages is regulated by adaptor proteins, which determine the site of assembly and control the size of the assembled cages (Brodsky, 1997; Keen, 1990).

The problem in the regulation of virus assembly is that multiple identical protein subunits must undergo conformational switching to correctly determine the size of the viral capsid. Regulated conformational switching is necessary because in the assembled capsid the subunit conformations are not all equivalent, with the number of different quasiequivalent conformations (known as the *T* number) determining the capsid size (Caspar and Klug, 1962). As each identical coat protein subunit is added to the capsid, a choice must be made as to which conformation the subunit will adopt. Various mechanisms for the regulation of conformational switching exist, including structural transitions in the regulatory regions of coat subunits and interactions of coat subunits with ordered nucleic acid within the capsid (Johnson, 1996). In the larger and more complex viruses, regulation is provided by binding interactions with another viral protein, the scaffolding protein.

Scaffolding protein-assisted assembly pathways are utilized by the herpesviruses and adenoviruses (D'Halluin et al., 1978; Edvardsson et al., 1976; Rixon, 1993), as well as the dsDNA bacteriophages (Casjens and Hendrix, 1988). The transient presence of scaffolding proteins is required during assembly to direct correct assembly of non-DNA-containing precursor capsids (known as procapsids). After assembly, scaffolding proteins are removed to allow DNA packaging to occur. In the absence of scaffolding proteins, assembly of the coat protein is slower (Earnshaw and King, 1978). In addition, most of the assembly products of both phage and herpesvirus coat proteins formed in the absence of the scaffolding protein are either aberrant spiral structures or smaller-than-normal capsids that are incapable of

Received for publication 30 November 1998 and in final form 22 March 1999.

Address reprint requests to Dr. Pamela A. Thuman-Commike, Department of Biochemistry, Baylor College of Medicine, One Baylor Plaza, Houston, TX 77030. Tel.: 925-417-0160; Fax: 650-932-1637; E-mail: pthuman@bcm.tmc.edu.

Dr. Malinski's present address is ATG Laboratories, 10300 Valley View Rd. #107, Eden Prairie, MN 55344.

Dr. Burbea's present address is Department of Molecular and Cell Biology, University of California Berkeley, Berkeley, CA 94720.

0006-3495/99/06/3267/11 $2.00

packaging DNA (Earnshaw and King, 1978; Matusick-Kumar et al., 1994; Ray and Murialdo, 1975; Roeder and Sadowski, 1977; Tatman et al., 1994; Thomsen et al., 1994).

The *Salmonella typhimurium* bacteriophage P22 provides a useful model system for understanding the assembly of the more complex animal viruses and possesses a well-developed in vitro assembly system (Prevelige et al., 1988, 1993b). Assembly of the P22 procapsid requires the copolymerization of ~200–300 scaffolding subunits with 420 molecules of coat protein. During assembly a dodecameric portal complex through which the DNA is packaged and 10–20 molecules of each of three pilot proteins required for DNA injection into the host cell are also incorporated. However, only the coat and scaffolding proteins are required for the assembly of procapsid-like particles.

Study of both the P22 and herpesvirus assembly pathways in vitro has determined that the scaffolding proteins do not form cores about which the coat proteins assemble; instead, assembly proceeds through the addition of both scaffolding and coat subunits to the edge of a growing shell (Newcomb et al., 1996; Prevelige et al., 1988). Despite the scaffolding protein's critical role in determining icosahedral symmetry, scaffolding was not observed in the structures of P22 procapsids (Thuman-Commike et al., 1996), herpesvirus procapsids (Trus et al., 1996), or herpesevirus B-capsids (Zhou et al., 1998a), suggesting that the bulk of the scaffolding protein lacks icosahedral symmetry.

Despite the lack of icosahedral symmetry in the bulk of the scaffolding protein, it remains possible that a portion of the scaffolding protein binds to specific sites within the icosahedral coat lattice. Such an icosahedrally ordered coat/scaffolding interaction could explain how scaffolding can cause conformational differences between coat subunits. To detect such interaction sites, we have determined and compared electron cryomicroscopy structures of scaffolding-containing and scaffolding-lacking procapsids. The resulting difference maps suggest that the scaffolding protein binds to a subset of coat subunits within the capsid lattice, supporting the idea that the conformational switching of a coat subunit is regulated by the type of interactions it makes with the scaffolding protein. Based on these results, we suggest a model for how the specific coat/scaffolding interactions may regulate procapsid assembly and size determination in both phage and animal viruses.

MATERIALS AND METHODS

Capsid preparation

Procapsids assembled in the absence of the scaffolding protein (gp5 procapsids) were prepared as previously described (Thuman-Commike et al., 1998). Procapsids lacking the pilot and portal proteins (gp5/8 procapsids) were prepared from cells infected with 1*am*H201/16*am*N121/20*am*N20/13*am*H101/c17 phage. Cell infection and procapsid purification were carried out essentially as previously described (Prevelige et al., 1988). Briefly, *S. typhimurium* strain DB7136 was infected at a multiplicity of infection of ~0.1 and allowed to grow at 37°C for ~4 h. Cells were harvested by centrifugation and lysed by repeated freeze/thawing, and cell debris was pelleted after treatment with DNase and RNase. The crude procapsids were harvested from the supernatant by centrifugation and purified by velocity sedimentation on a 5–20% sucrose gradient. Fractions containing procapsids were identified both visually by turbidity and by sodium dodecyl sulfate-polyacrylamide gel electrophoresis (SDS-PAGE). Appropriate fractions were pooled, washed, and concentrated by sedimentation.

GuHCl extraction of procapsids

Scaffolding protein was removed from the gp5/8 procapsids by treatment with 0.5 M GuHCl as previously described (Prasad et al., 1993). Briefly, purified procapsids were made in 0.5 M GuHCl, 50 mM Tris, 25 mM NaCl, and 2 mM EDTA at pH7.0. This treatment releases the scaffolding protein and leaves intact the shells of coat protein. The coat protein shells were separated from the released scaffolding protein by pelleting in an ultracentrifuge. Pelleted shells were resuspended in 0.5 M GuHCl, and the process was repeated. Extraction was continued until the scaffolding protein was fully removed as monitored by SDS-PAGE, typically for three cycles. GuHCl treatment of the gp5 procapsids was performed in the same manner, with three extraction cycles.

Electron cryomicroscopy

Capsid samples were applied to copper grids covered with holey carbon film (Fukami and Adachi, 1965; Toyoshima, 1989). After removal of excess solution by blotting, grids were rapidly plunged into liquid ethane (Adrian et al., 1984; Dubochet et al., 1988). Vitrified samples were stored under liquid nitrogen until they were transferred into a JEOL 1200 microscope equipped with a Gatan 651-N anticontaminator, maintained at −179°C, and a Gatan 626 cold stage, maintained at −165°C. Flood-beam images were obtained with 100-kV electrons at a magnification of 30,000× under low-dose conditions (less than or equal to 5 $e^-/Å^2$). Kodak SO-163 film was used to record images, which were developed in full-strength Kodak D19 for 12 min at 20°C and fixed for 10 min in Kodak fixer.

Image analysis and three-dimensional reconstruction

All capsids were processed similarly to the previously determined procapsids assembled in the absence of the scaffolding protein (Thuman-Commike et al., 1998). Electron micrographs were visually inspected for quality, and the close-to-focus images of suitable micrographs were scanned with a Perkin-Elmer 1010M microdensitomer with a step size of 17 μm, corresponding to 5.57 Å per pixel. Particle selection was performed using automated reference-based particle selection (Thuman-Commike and Chiu, 1995; Thuman-Commike and Chiu, 1996). The selected particles were perimeter average subtracted and extracted as 128 × 128 pixel images. Image defocus and quality were analyzed by computing the sum of the particle image Fourier transform intensities (Zhou et al., 1996).

Particle center and angular parameters were estimated using cross-correlation and several modified versions of the self-common lines function (Crowther et al., 1970; Fuller, 1987; Thuman-Commike and Chiu, 1997). Initial sets of orientations were identified using a cross-common lines phase residual comparison between a set of computed projection images (Crowther et al., 1994; Zhou et al., 1994) generated from the previously published 19-Å scaffolding mutant procapsid reconstruction (Thuman-Commike et al., 1996). After determination of the initial orientations, projection images were computed from the low-resolution structures to determine additional particle orientations, using the cross-common lines phase residual comparison.

The final resolution of each reconstruction was verified by the icosahedral cross-common lines phase residual (Crowther, 1971), the Fourier ring correlation coefficient (Radermacher, 1988; van Heel, 1987), and the amplitude-weighted mean phase difference (Baker et al., 1990; Frank et al., 1981). Adequate Fourier space sampling was ensured by calculating the inverse eigenvalue spectrum during the interpolation step of the Fourier-Bessel analysis of the final reconstructions (Crowther, 1971; Crowther et

al., 1970). Full icosahedral symmetry was obtained for the final reconstructions by imposing real space threefold averaging (Fuller, 1987). Furthermore, to ensure accurate and interpretable difference maps, all reconstructions were determined from images obtained under comparable conditions (0.9–1.1 μm underfocus) and were all determined to 22-Å resolution.

Difference maps

Several types of difference maps were computed to confirm and substantiate the observed results. The simplest difference map calculated was the algebraic difference between all corresponding points in the reconstructions for which the density was at or above the contour threshold level (Marvik et al., 1995). This algebraic difference was performed on maps both with and without radial and/or density scaling. The radial and density scaling were performed by comparison of the spherically averaged radial density profile for each of the corresponding maps within the range of the coat protein shell (Booy et al., 1994; Lawton and Prasad, 1996; Venien-Bryan and Fuller, 1994). In each of these cases, differences were considered statistically significant if they were present at 3σ above the mean density in the difference map. In addition to the algebraic difference maps, Student's t-test ($n = 9$) was used to confirm statistically significant structural differences (McGough et al., 1994; Milligan and Flicker, 1987; Trachtenberg and DeRosier, 1987). All significant difference densities were consistent between the various types of computed difference maps. For simplicity, we have opted to show the observed results by superimposing the algebraic difference map on the three-dimensional structure.

RESULTS

Scaffolding-lacking and scaffolding-containing procapsids

Our approach to isolating the location of the coat/scaffolding interface was to compute difference maps between structures of scaffolding-containing and scaffolding-lacking procapsids. The wild-type procapsid, however, contains not only the coat protein, gp5, and the scaffolding protein, gp8, but also the portal protein, gp1, and the three pilot proteins, gp7, gp16, and gp20 (Fig. 1 *A*). Thus, using the wild-type procapsid may result in misinterpretation of the difference maps due to the presence of the additional proteins. Consequently, we have purified 1-/16-/20- procapsids, subsequently referred to as gp5/8 procapsids, for use as the scaffolding-containing procapsids. As shown in Fig. 1 *B*, the gp5/8 procapsids contain gp5 and gp8 but do not appear to contain gp1, gp16, or gp20. We should note that these capsids might contain the minor pilot protein gp7. However, even if gp7 is present in these procapsids, gp7 is a small 18-kDa protein (King et al., 1973) with only 10–12 copies in the procapsid; therefore it is unlikely that the possible presence of gp7 could affect our results. For procapsids lacking the scaffolding protein, we have purified both procapsids assembled in the absence of the scaffolding protein, subsequently referred to as gp5 procapsids and gp5/8 procapsids treated with GuHCl, which causes release of the scaffolding protein (Fuller and King, 1981). As previously determined (Earnshaw and King, 1978; Thuman-Commike et al., 1998), the gp5 procapsids lack the scaffolding protein and do not appear to contain the portal protein, gp1, or either of the two pilot proteins, gp16 and gp20. Similarly, after GuHCl treatment the gp5/8 procapsids no longer contain the scaffolding protein (Fig. 1 *C*).

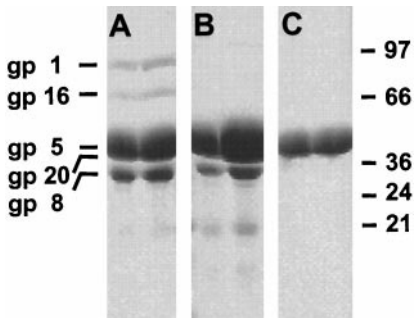

FIGURE 1 Protein composition of wild-type and gp5/8 P22 procapsids. Procapsid samples were analyzed by SDS-PAGE on a 12% polyacrylamide gel stained with Coomassie blue. (*A*) Wild-type procapsids. (*B*) gp5/8 procapsids. (*C*) gp5/8 procapsids treated with GuHCl. The right lane of each panel contains twice the amount of protein in the left lane. Positions of the P22 coat protein (gp5), scaffolding protein (gp8), portal protein (gp1), and pilot proteins (gp16 and gp20) are shown.

Procapsid structure

The bacteriophage P22 procapsid forms a $T = 7$ icosahedral capsid with an outer shell composed of seven quasiequivalent coat subunits (Prasad et al., 1993; Thuman-Commike et al., 1998, 1996). The procapsid shell has an average radius of 280 Å and a maximum radius of 306 Å. Fig. 2 demonstrates the overall structural features of the inner and outer coat surface of the gp5/8 procapsid. Note that although the gp5/8 procapsid was chosen for this demonstration, all of the determined procapsid structures have the same overall structural features. The outer procapsid surface is composed of penton and skewed hexon clusters, each with a central channel (Fig. 2, *A* and *C*). In addition, the outer coat surface has valleys at all strict and local threefold axes (Fig. 2, *A* and *C*) and saddle-like regions present between pairs of hexon-penton and hexon-hexon subunits (Fig. 2, *A* and *C*). The procapsid inner coat surface is composed of trimer clusters at all strict and local threefold axes (Fig. 2, *B* and *D*) that correspond to the positions of the valleys observed on the outer surface. Located between the trimer clusters is a network of grooves (Fig. 2, *B* and *D*) that correspond to the positions of the saddle-like regions observed on the outer surface. The presence of internal density differs in all structures; however, when present; all internal density is non-icosahedral, as determined by comparison of the threefold and nonthreefold averaged reconstructions (Thuman-Commike et al., 1996). Consequently, the internal density will not be considered in any of the remaining analyses.

Coat/scaffolding interaction

Difference maps between gp5/8 and gp5 procapsids contain significant differences on the inner surface of the gp5/8 procapsid that are absent from the inner surface of the gp5

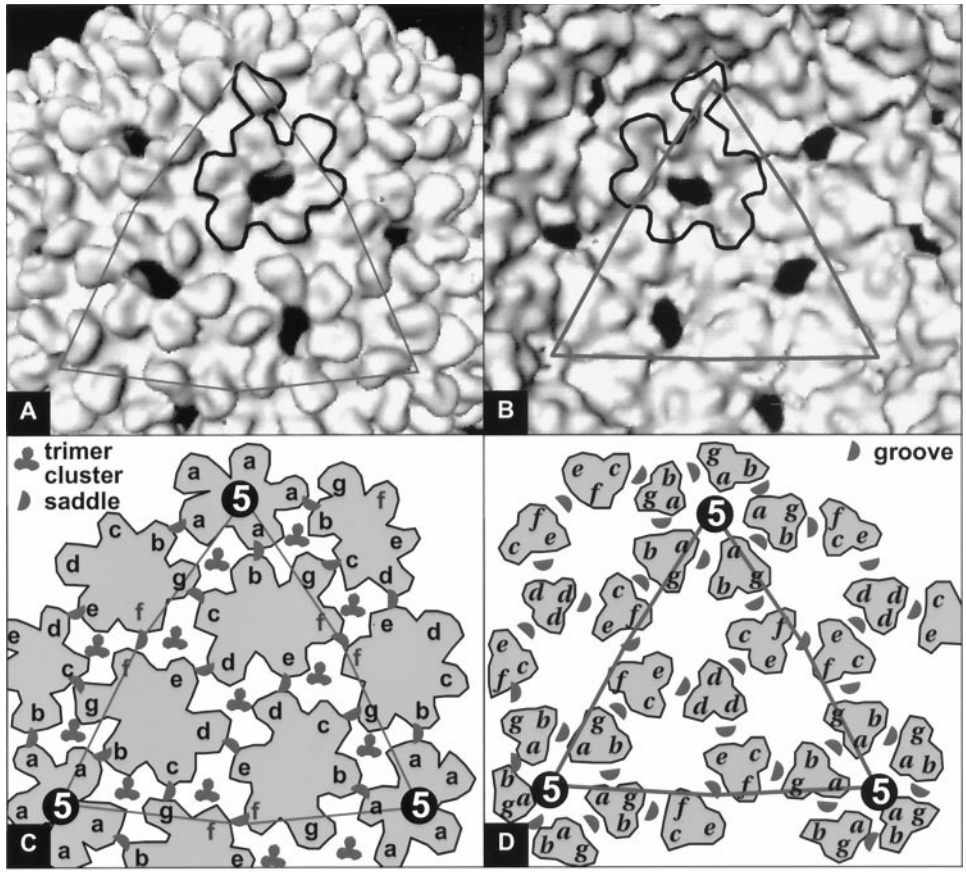

FIGURE 2 Overview of the main structural features in the bacteriophage P22 procapsid. (*A* and *B*) Surface representation of the 22 Å gp5/8 procapsid reconstruction: (*A*) outer surface and (*B*) inner surface. The footprints of the unit triangle and asymmetrical unit are shown as reference points. (*C* and *D*) Schematic of structural features present on the outer and inner procapsid surfaces. The seven unique quasiequivalent subunits are labeled *a*–*g*. (*C*) On the outer surface, the shaded regions represent the pentons and skewed hexons. The locations of the triangular pits are marked by clovers at all strict and local threefold axes. In addition, the locations of the saddle-like regions between pairs of hexon-hexon and hexon-penton subunits are marked by half-circles. (*D*) On the inner surface, shaded regions represent the triangular clusters that compose the inner surface at all strict and local threefold axes. The locations of the grooves, which correspond to the saddle-like regions between pairs of hexon-hexon and hexon-penton subunits on the outer surface, are marked by the half-circles.

procapsid (Fig. 3 *A*). These differences appear as a cluster of four densities at the trimer tips of the b, c, f, and g subunits (Fig. 3 *A*, *circled densities*). These four densities are the only significant difference densities between these two structures. Consequently, we attribute the four densities at the trimer tips of the b, c, f, and g subunits to the points of interaction between the coat and the scaffolding protein in the procapsid (Fig. 3 *C*). The small amount of observed difference density attributed to the scaffolding protein suggests that the scaffolding is only icosahedrally ordered for a small distance within the coat protein shell. Consistent with this notion is evidence that the 30 C-terminal amino acids required for binding of the coat protein are helical (Tuma et al., 1998), but that the region immediately adjacent to this region is flexible (Prevelige, unpublished observations). This flexibility could account for the rapid decay of icosahedral order.

We should note that these locations differ from our previously proposed (Thuman-Commike et al., 1996) location of the coat/scaffolding interaction that was based solely on the structural appearance of the inner procapsid surface. In the current study, we have based our assignment of the coat/scaffolding interaction on differences observed between scaffolding-containing and scaffolding-lacking procapsids. This assignment of the b, c, f, and g subunits is consistent with all current data regarding the scaffolding protein. Binding of a single scaffolding molecule at each of the b, c, f, and g subunits of the capsid would result in a total of 240 scaffolding molecules within the procapsid, in accordance with previous estimates (Casjens and King, 1974). Furthermore, analytical ultracentrifugation of purified scaffolding protein has demonstrated that the scaffolding subunits interact with each other to form dimers and tetramers (Parker et al., 1997). From the relative positions of the identified interaction sites, the scaffolding subunits are located ~50 Å apart and could easily form both dimeric and tetrameric interactions. By making these interactions, the scaffolding subunits link adjacent hexamers to each other as viewed from the outside, and adjacent trimers as seen from the inside, thus helping to cement together the coat subassemblies within the capsid. The presence of scaffolding tetramers has also been observed for the external scaffolding gpSid of P4 (Marvik et al., 1995) and the external scaffolding gpD of ϕX174 (Dokland et al., 1997; Ilag et al., 1995). Although these procapsids each have different underlying coat/scaffolding interactions, the appearance of scaffolding tetramers appears to be a recurring theme.

To further confirm the point of interaction between the coat and scaffolding protein, we compared the gp5/8 procapsid before and after GuHCl treatment. Several distinct regions of significant difference were observed in this comparison. Examination of the differences attributed to the gp5/8 procapsid at the inner surface reveals densities at the trimer tips of the c and f subunits (Fig. 3 *B*, *circled densi-*

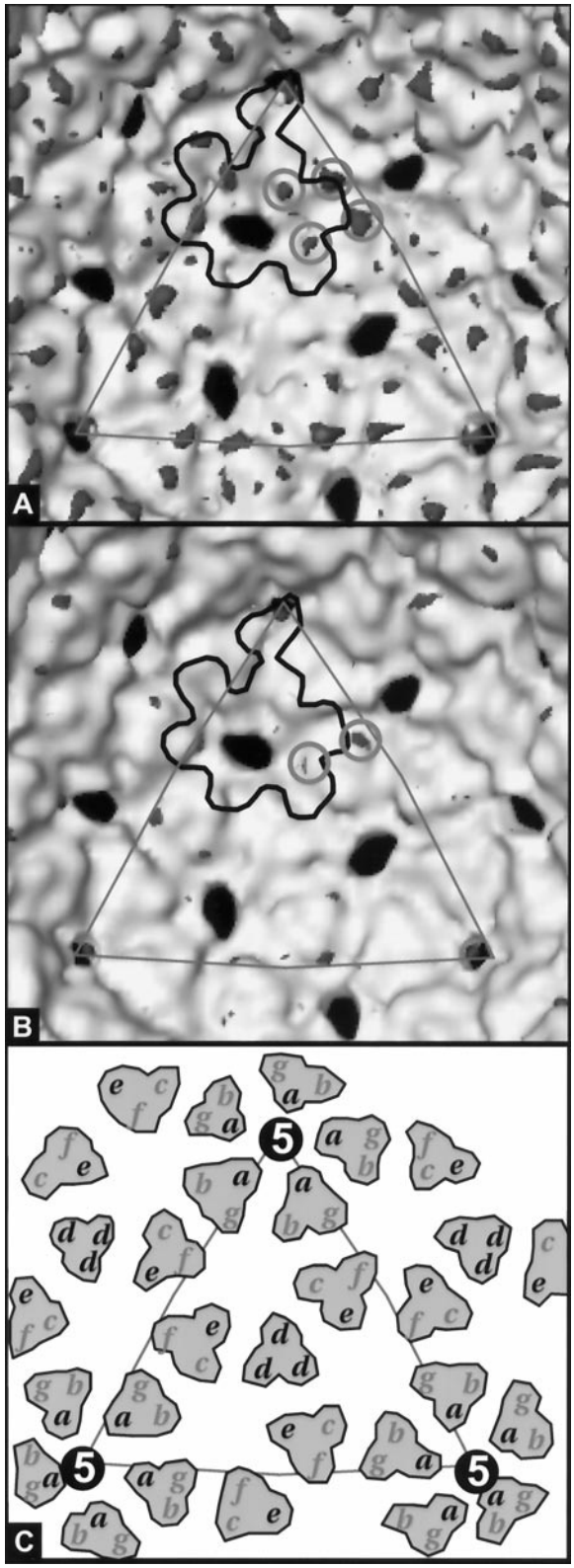

FIGURE 3 Localization of the coat/scaffolding interface. (*A*) Difference imaging between the gp5/8 and gp5 procapsids. The surface representation of the gp5 procapsid is shown in white, and the difference map representing features present in the gp5/8 procapsid but absent from the gp5 procapsid is shown in red. The four circled densities correspond to the density attributed to the coat/scaffolding interaction at the trimer tips of the b, c, f, and g subunits. (*B*) Difference imaging between the gp5/8 and GuHCl-treated gp5/8 procapsids. The surface representation of the GuHCl-treated gp5/8 procapsid is shown in white, and the difference map representing features present in the gp5/8 procapsid but absent from the GuHCl-treated gp5/8 procapsid is shown in red. That is, the red density is the positive difference between the gp5/8 procapsid and the GuHCl-treated gp5/8 procapsid. The circled densities correspond to the density attributed to the coat/scaffolding interaction at the trimer tips of the c and f subunits. (*C*) Cartoon schematic denoting the identified locations of the coat/scaffolding interaction. Subunits labeled in red interact with scaffolding, and subunits labeled in black do not interact with scaffolding.

ties). No other significant difference is present on the inner surface. Thus we interpret these two densities as points of interaction between the coat and the scaffolding protein. These densities are consistent with the densities observed on the c and f subunits in the comparison with the gp5 procapsids (Fig. 3 *A*). In the comparison of GuHCl-treated gp5/8 procapsids, however, we observe differences only at the trimer tips of the c and f subunits (Fig. 3 *B*). The densities at the b and g trimer tips are still present in the GuHCl-treated gp5/8 procapsid. This might suggest that only half of the scaffolding molecules (at the c and f subunits) are extracted by the GuHCl treatment, whereas those bound to the b and g subunits remain. Assignment of the scaffolding to the densities at the b and g trimer tips, however, is inconsistent with the SDS-PAGE of the GuHCl-treated gp5/8 procapsids (Fig. 1), which shows that the scaffolding is totally absent. Therefore, it is unlikely the densities at the b and g trimer tips are scaffolding protein.

An alternative explanation is that the observed density at the trimer tips is derived from the presence of an alternative coat protein conformation because the coat subunits that interact with scaffolding must adopt an altered conformation in which a scaffolding binding site is presented on the inner capsid surface. In this case, extraction of the scaffolding protein by GuHCl would cause the c and f subunits to revert back to a conformation that lacked the binding site, whereas the b and g subunits would remain in the scaffolding-binding conformation, even in the absence of scaffolding protein. This model is consistent with previous evidence indicating that the procapsid contains two classes of scaffolding binding sites with different affinities for scaffolding protein subunits (Greene and King, 1994).

Consequences of GuHCl treatment

Comparison of the gp5/8 procapsid before and after GuHCl treatment reveals not only positive differences at the inner surface attributed to the gp5/8 procapsid (Fig. 3 *B*), but also positive differences at the outer surface attributed to the gp5/8 procapsid (Fig. 4 *A*) and negative differences at the inner surface attributed to the GuHCl-treated procapsid (Fig. 4 *B*). Several difference densities are observed on the outer coat surface of the GuHCl-treated gp5/8 procapsids that are attributable to the gp5/8 procapsid (Fig. 4 *A*). These differences include a number of relatively small densities at the tips of most of the hexon and penton petals and densities in the saddle-like regions between the hexon-hexon subunits

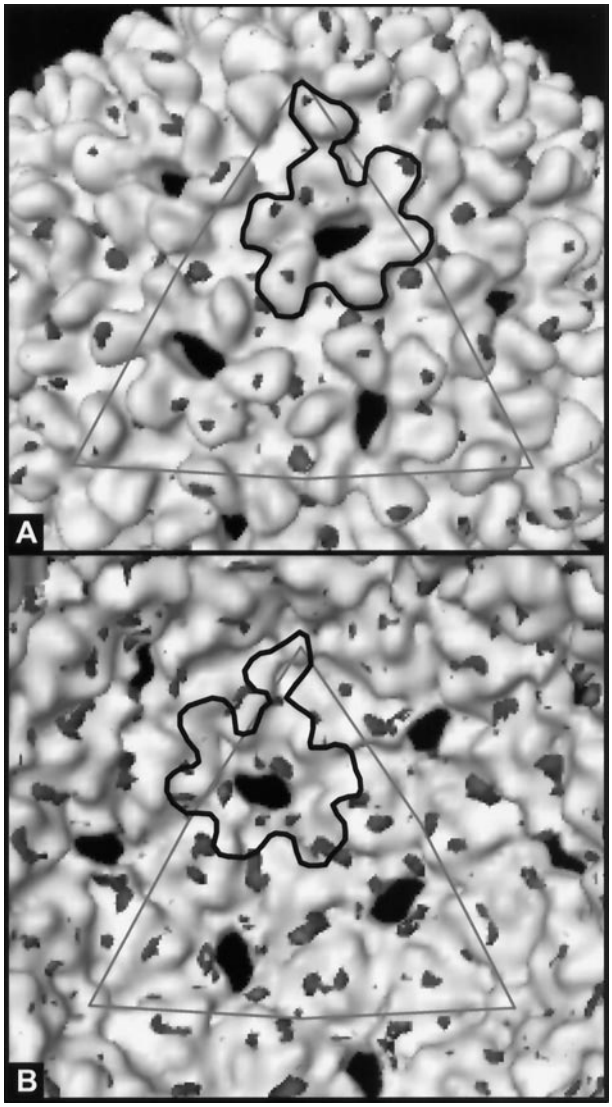

FIGURE 4 Difference imaging revealing the consequences of GuHCl treatment for procapsids. (*A*) Outer surface representation of differences present in the gp5/8 procapsid before but not after GuHCl treatment. The surface representation of the GuHCl-treated gp5/8 procapsid is shown in white, and the difference map is shown in red. Difference densities are at or near the tip of the penton and hexon subunits and in the saddle-like regions between the d-e and f-f subunits. (*B*) Inner surface representation of features present in the GuHCl-treated gp5/8 procapsid but absent in the gp5/8 procapsid before GuHCl treatment. The surface representation of the gp5/8 procapsid is shown in white, and the difference map is shown in red. Difference densities are present on the grooves surrounding the icosahedral threefold axis, on the trimer clusters, and surrounding the hexon holes. Note that the red density in *B* is the negative difference between the gp5/8 procapsid and the GuHCl-treated gp5/8 procapsid, whereas the red density in Fig. 3 *B* is the positive difference.

e-d and f-f (Fig. 4 *A*). These differences suggest that the petals and saddle-like regions of the gp5/8 procapsid extend outward slightly more than those in the GuHCl-treated gp5/8 procapsid.

Difference maps between gp5/8 procapsids before and after GuHCl treatment also identify several densities present on the inner surface of the GuHCl-treated gp5/8 procapsid that are absent in the gp5/8 procapsid (Fig. 4 *B*). The principal difference occurs in the grooves surrounding the strict icosahedral threefold axis, with other, weaker differences surrounding the hexon holes and in the center of the flat region of the trimer clusters (Fig. 4 *B*). These differences complement the differences attributed to the outer surface of the gp5/8 procapsid (Fig. 4 *A*) and further suggest that an inward flattening movement has occurred to the procapsid after chemical treatment.

To determine whether the observed structural changes are a result of the GuHCl treatment or scaffolding release, we compared the gp5 procapsid before and after GuHCl treatment (results not shown). The resulting difference maps also suggest that an inward movement has occurred to the procapsid after GuHCl treatment. Because the gp5 procapsid does not contain scaffolding protein, these results confirm that the inward movement is a result of the chemical treatment and not the exit of the scaffolding protein.

We interpret the observed inward movement of GuHCl-treated procapsids as a possible mimic of an initial step in the maturation transition. Maturation requires release of the scaffolding protein (Greene and King, 1996; King and Casjens, 1974), followed by flattening of the icosahedral lattice and an overall expansion of the capsid (Prasad et al., 1993). The differences we observe result in a flattening of the capsid, which is consistent with maturation flattening, suggesting that we may be observing an intermediate in capsid maturation.

DISCUSSION

Procapsid assembly models

Our difference maps suggest specific interactions of scaffolding protein with only four of the seven quasiequivalent coat protein conformations in the P22 procapsid lattice (Fig. 3 *C*). These interactions further suggest that scaffolding protein can form dimers and tetramers within the procapsid. We propose a model for P22 procapsid assembly that involves self-association of both coat and scaffolding subunits, as well as specific interactions between the two proteins. During assembly coat protein subunits are recruited from a pool of subunits in an undefined conformation and are subsequently switched to the correct one of seven quasiequivalent conformations, based upon their interactions with neighboring coat and scaffolding subunits in the growing capsid. In this model, assembly is not driven primarily by the scaffolding; instead, assembly involves alternating steps in which first coat, then scaffolding subunits form self-interactions and then catalyze the addition of the other protein. Together, the coat and scaffolding provide overlapping sets of binding interactions that drive formation of the procapsid.

We propose that the first step in procapsid assembly, as suggested by the kinetics of P22 in vitro assembly, is the formation of a coat pentamer (Prevelige et al., 1993a). Within infected cells, procapsid initiation also involves the

participation of the portal complex, which may form a larger complex including the pilot proteins as well as coat and scaffolding subunits. Thus the first step in procapsid assembly may also involve the addition of coat and scaffolding subunits to form the first ring of trimers, with scaffolding bound to coat subunits in the b and g conformations (Fig. 5, *A* and *A′*). The next coat subunits to be added must initiate a new ring of trimer clusters, while not yet being able to complete the hexons. An insufficiency of favorable binding interactions at this stage could make it difficult for these

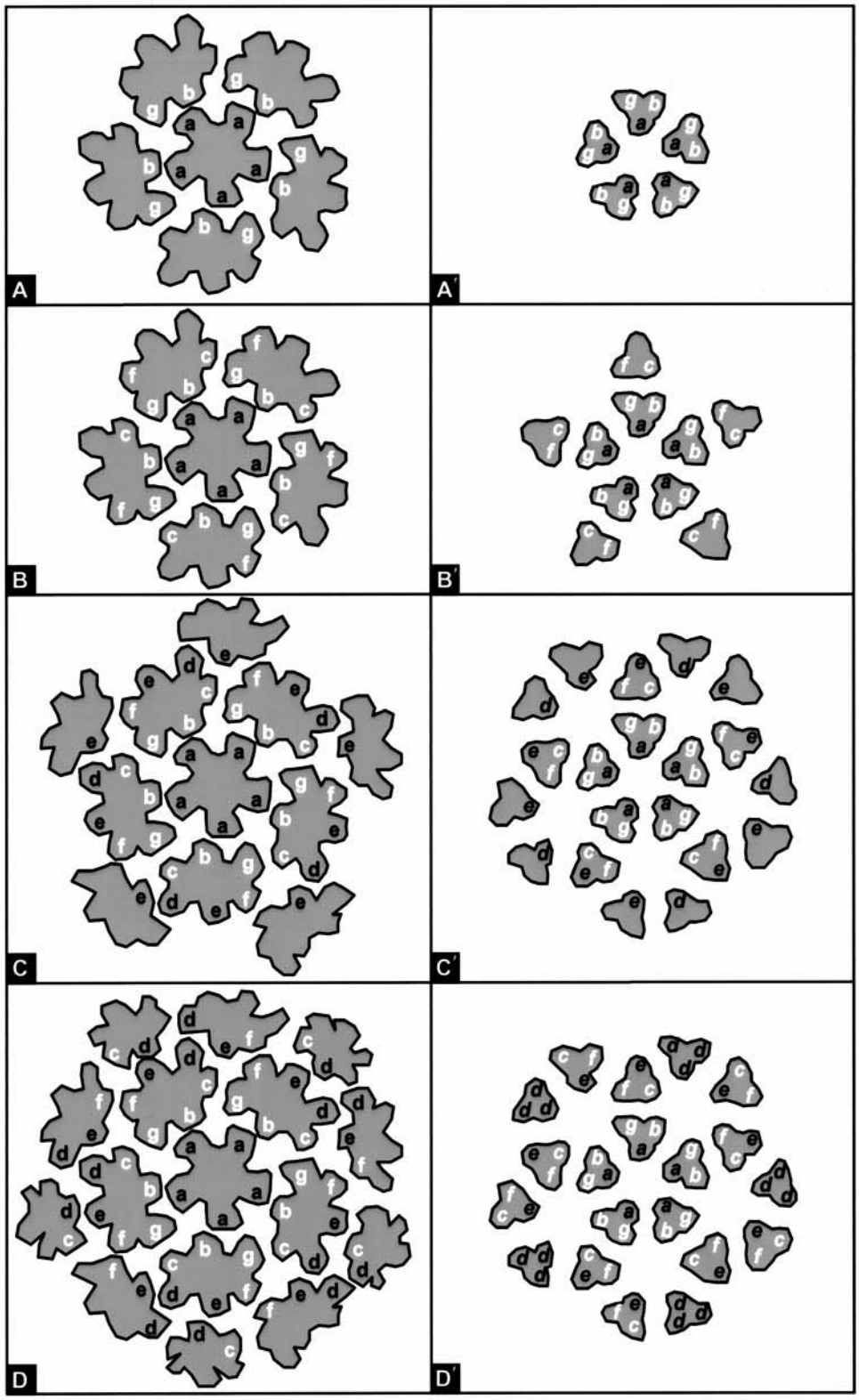

FIGURE 5 Schematic of the scaffolding-directed procapsid assembly model. In this schematic, trimers, hexons, and pentons are only completely assembled when all subunit labels have been added, although the entire outline is present from the time any individual subunit is added. Subunits labeled in white have scaffolding bound, and subunits labeled in black do not interact with scaffolding. The left column views assembly from the outside of the capsid, and the right column views assembly from the inside of the capsid. (*A*, *A′*) Initial assembly occurs at the fivefold symmetry axis. Either during or after formation of the penton, additional subunits add to form complete trimer clusters surrounding each penton. (*B*, *B′*) Coat and scaffolding subunit addition then proceeds, driven by tetrameric scaffolding interactions. (*C*, *C′*) At this point a number of coat subunits are added, driven by completion of trimers, on the inner surface, and by completion of hexons, on the outer surface. (*D*, *D′*) Next, the addition of more coat subunits results in completion of the ddd and cef trimers on the inner surface. The addition of these subunits also results in the opening of scaffolding interaction locations at the coat subunits in the c and f conformations. Coat and scaffolding subunit addition then proceeds, driven by tetrameric scaffolding interactions, resulting in the addition of coat subunits that switch to the b and g conformations, after which the assembly process continues.

coat subunits to stably attach to the shell. We suggest that this step is therefore driven by the binding interactions of the scaffolding subunits, which can form tetrameric clusters with the scaffolding subunits that bind to the c and f coat subunits (Fig. 5, *B* and *B′*). After this step, the next coat subunits to bind would complete the first ring of hexons (Fig. 5 *C*) and another set of trimer clusters (Fig. 5 *C′*). Completion of another set of trimeric interactions could drive the addition of the next set of coat subunits (Fig. 5 *D′*). At this stage, scaffolding molecules must be driven to bind to the newly added coat subunits in the c and f, but not the d and e conformations. It may be significant that of these newly added subunits, those in the f position are the closest to any subunit that already has scaffolding bound (Fig. 5 *D*). By contact with these scaffolding-bound subunits, the newly added subunits in the f position might be induced to shift to a scaffolding-binding conformation. Alternatively, the conformations of the d and e subunits may already have been set, by their interactions within the skewed hexon ring, to conformations incapable of binding scaffolding. Once scaffolding has bound to both the f and c subunits, addition of the coat subunits that switch to the b and g conformations, and so on, could proceed through the steps described above.

In this model the scaffolding serves to help the assembly of the coat shell over the "difficult" steps. That is, at those steps for which addition of coat subunits does not complete enough binding interactions to provide sufficient energy for stable coat subunit addition, interactions between scaffolding subunits provide the motivating force. This model would predict that a high enough concentration of coat protein could favor the completion of even the difficult assembly steps, but that the presence of scaffolding would significantly lower the critical concentration of coat protein required for procapsid assembly, as is, in fact, the case (Prevelige et al., 1993a).

Conformational switching and size regulation

Given the above model describing the assembly steps in procapsid formation, the next question is how to ensure that the assembled capsid has the proper size. Assembly of a properly sized capsid requires each viral coat subunit to adopt the correct one of multiple quasiequivalent conformations, depending upon the *T* number of the capsid. The coat protein by itself must be able to provide some regulation of procapsid size, because the coat proteins of the $T = 7$ phages seem intrinsically capable of forming both $T = 7$ and $T = 4$ capsids but not capsids of larger or smaller *T* numbers. For example, capsids made by P22 coat protein in the absence of scaffolding (Earnshaw and King, 1978), by mutant λ coat proteins (Katsura, 1983), and by P2 coat protein in the presence of the parasitic P4 protein gpSid (Dokland et al., 1992) are all $T = 4$ instead of the correct $T = 7$. Capsids with *T* numbers of 3, 9, or 12 have never been observed in these systems. Similarly, herpesvirus coat protein in the absence of scaffolding and one of the triplex proteins forms $T = 7$ capsids (Saad, Zhou, Jakana, Chiu, and Rixon, unpublished observations).

One property that seems likely to contribute to the size-regulating ability of coat proteins is the propensity to form skewed hexon clusters. The hexons within procapsids of the dsDNA phages P22 (Prasad et al., 1993), λ (Dokland and Murialdo, 1993), and HK97 (Conway et al., 1995), as well as the herpesvirus procapsid (Trus et al., 1996), all show pronounced deviations from the sixfold symmetry present in the mature viruses. Surprisingly, the structures of the $T = 7$ and $T = 4$ P22 capsids formed in the absence of scaffolding protein revealed that both contained hexons with the same skewed structure (Thuman-Commike et al., 1998); thus at least for P22, hexon skewing is not sufficient to determine the choice of $T = 7$ versus $T = 4$ structures. However, because a hexon with only twofold symmetry must contain either three or six different conformations, the *T* number of a capsid in which all hexons are skewed must be $3n + 1$. Thus the coat protein by itself, because of its propensity to form skewed hexons, limits the possible structures to $T = 4$, 7, 13, 16, and so forth. These limited *T* numbers correspond to those actually observed for these viruses, from the $T = 7$ and $T = 4$ phage capsids discussed above to the $T = 13$ bacteriophage T4 capsid (Black et al., 1994) and the $T = 16$ herpesvirus capsids (Schrag et al., 1989).

An additional regulatory property of the coat protein is its potential for binding interactions with the scaffolding protein, which presumably further limits the choice of capsid size to the single correct *T* number for each virus. It is possible to propose simple rules of P22 scaffolding binding interactions that can direct $T = 7$ formation and prevent the assembly of capsids of incorrect *T* numbers. In this discussion, it is assumed that the scaffolding dimer interactions are formed between scaffolding molecules bound to coat subunits b–g and c–f, whereas interactions between scaffoldings bound to b–c and g–f coat subunits occur only after the formation of tetramers.

The first problem in building a $T = 7$ procapsid is preventing the formation of a $T = 4$ capsid. A rule to prevent this, as suggested by our localization of the coat/scaffolding interface, is that scaffolding subunits can bind only two out of three coat subunits in a single trimer cluster. This may be because binding of scaffolding to the coat is stabilized by dimeric interactions with an adjacent scaffolding subunit; once two subunits have bound to a trimer cluster, a third scaffolding subunit would have no available partner with which to form the stabilizing dimer interaction, and thus would not remain bound. Consistent with this suggestion, in vitro assembly experiments with both truncated and full-length scaffolding proteins indicate that each P22 scaffolding dimer must be able to bind two coat subunits to participate in assembly (Parker et al., 1998). As shown in Fig. 6 *A*, formation of a $T = 4$ lattice requires a threefold interaction of the c subunits. In the P22 lattice (Fig. 6 *B*), however, scaffolding protein binds two of those subunits (designated c and f), and because a third scaffold-

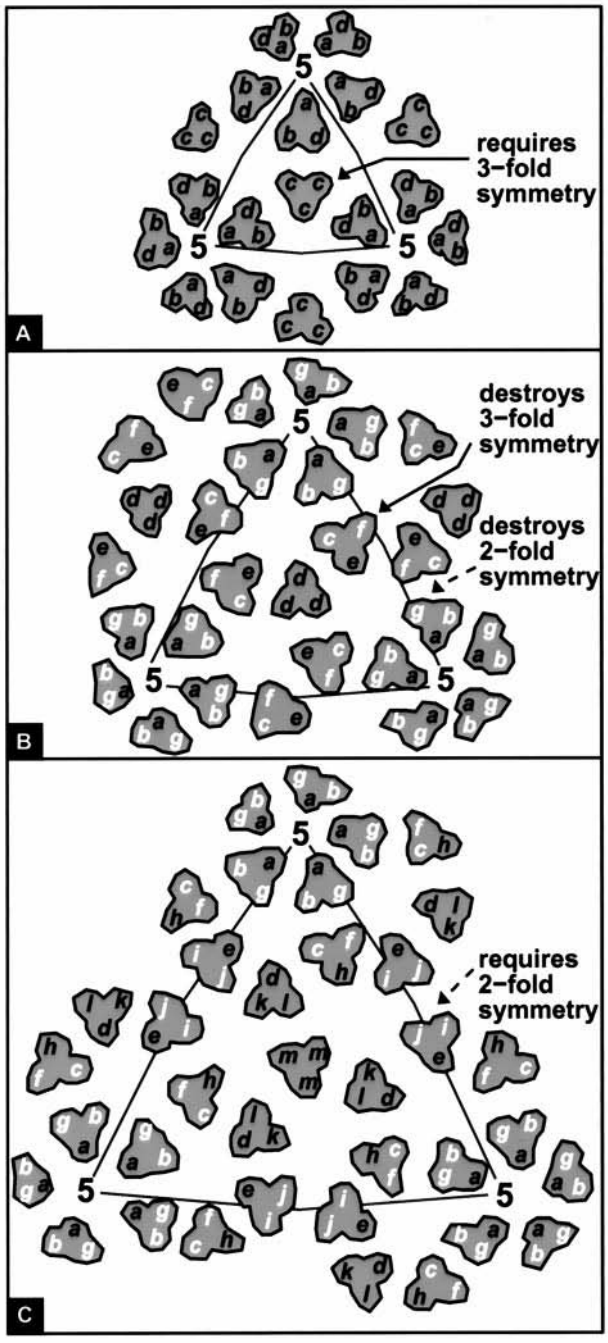

FIGURE 6 Role of the scaffolding protein in capsid size determination. Shown are schematics of (*A*) $T = 4$, (*B*) $T = 7$, and (*C*) $T = 13$ icosahedral lattices viewed from the inside. Subunits with scaffolding bound are shown in white, and subunits without scaffolding bound are shown in black. Notice that binding of scaffolding prevents the formation of the threefold symmetry axis of the $T = 4$ lattice and the twofold symmetry axis of the $T = 13$ lattice.

ing protein cannot be bound to the trimer, the threefold symmetry is irrevocably destroyed, eliminating the possibility of forming a $T = 4$ shell.

The other problem that must be addressed is preventing the formation of capsids with T numbers greater than 7 and preventing the formation of unclosed spiral structures, which can result from failing to form pentamers at the correct sites (Berger et al., 1994). As shown in Fig. 6, *B* and *C*, in a $T = 13$ capsid, what would be the second cf/bg interaction is, in a $T = 7$ capsid, a locus of twofold symmetry, with the subunits designated ij/ij in the $T = 13$ capsid. The ij/ij interaction would be prevented if the scaffolding tetramer did not possess twofold symmetry. This suggestion is supported by the recently determined structure of the external scaffolding protein of ϕX174, gpD (Dokland et al., 1997). gpD also forms tetramers, although in contrast to the P22 scaffolding, gpD binds to the outside of the capsid, and because the ϕX174 capsid is $T = 1$, each gpD subunit does not bind a separate coat subunit. The gpD tetramer consists of a dimer of dimers. Although the two dimers are almost identical, their binding interface is skewed such that the tetramer lacks twofold symmetry (Dokland et al., 1997). If the P22 scaffolding protein forms a similar tetramer, the difference in the angle of the two dimer halves could be such as to ensure that the b and g subunits are forced into a tighter conformation for the incorporation of a pentamer. Chemical cross-linking evidence indicates that the scaffolding tetramer, like gpD, is composed of a dimer of dimers (Parker and Prevelige, unpublished observations). The importance of tetrameric interactions is confirmed by the fact that scaffolding fragments incapable of forming tetramers direct the assembly of primarily aberrant spiral structures rather than closed capsids (Parker et al., 1998). It is also likely that both the intrinsic curvature of the coat protein and the constraints imposed by interactions of elongated scaffolding molecules within the capsid would prevent the formation of very large capsids.

Regulated self-assembly by different accessory proteins, including scaffolding, may also be involved in the formation of the larger herpesvirus and adenovirus capsids. The location of the herpesvirus scaffolding protein was observed in the B capsid (Zhou et al., 1998), although the precise sites of binding are not clear. Nonetheless, it is evident that as with P22, the herpesvirus scaffolding binds only to a subset of the quasiequivalent coat subunits present in the $T = 16$ virion (Zhou et al., 1998b). The triplex proteins also make nonequivalent interactions with the different coat subunits (Zhou et al., 1998b) and may provide the additional control required to prevent assembly of all possible capsids smaller than $T = 16$, given that in the absence of scaffolding and one of the triplex proteins, vp23, $T = 7$ capsids are formed (Saad, Zhou, Jakana, Chiu, and Rixon, unpublished observations). The assembly pathways of the $T = 25$ adenoviruses are not known in detail, but do involve scaffolding proteins (Cepko and Sharp, 1982; D'Halluin et al., 1978; Edvardsson et al., 1976). Moreover, the mature adenovirus virions contain additional structural proteins, including a specialized penton protein, a triplex protein, and two proteins that bind at other unique hexon interfaces (Stewart et al., 1993), all of which presumably add still more layers of regulation to form this still larger capsid.

The authors thank Dr. Jonathan King for helpful discussions and Mr. Kenneth French for preparation of the GuHCl-treated gp5 procapsids.

The W. M. Keck Foundation, the National Center for Research Resources of the National Institutes of Health (RR02250), the National Science Foundation (NSFBIR-9413229), and the National Institutes of Health (AI43656 to WC and AI38469 and GM47980 to PEP) supported this work. JAM thanks Dr. Theodore G. Wensel for his generous support (EY07981).

REFERENCES

Adrian, M., J. Dubochet, J. Lepault, and A. W. McDowall. 1984. Cryo-electron microscopy of viruses. *Nature.* 308:32–36.

Baker, T. S., W. W. Newcomb, F. P. Booy, J. C. Brown, and A. C. Steven. 1990. Three-dimensional structures of maturable and abortive capsids of equine herpesvirus 1 from cryoelectron microscopy. *J. Virol.* 64: 563–573.

Berger, B., P. W. Shor, L. Tucker-Kellogg, and J. King. 1994. Local rule-based theory of virus shell assembly. *Proc. Natl. Acad. Sci. USA.* 91:7732–7736.

Black, L. W., M. K. Showe, and A. C. Steven. 1994. Morphogenesis of the T4 head. *In* Molecular Biology of Bacteriophage T4, 2nd Ed. J. D. Karam, editor. ASM Press, Washington, DC. 218–258.

Booy, F. P., B. L. Trus, W. W. Newcomb, J. C. Brown, J. F. Conway, and A. C. Steven. 1994. Finding a needle in a haystack: detection of a small protein (the 12-kDa VP26) in a large complex (the 200-MDa capsid of herpes simplex virus). *Proc. Natl. Acad. Sci. USA.* 91:5652–5656.

Brodsky, F. M. 1997. New fashions in vesicle coats. *Trends Cell Biol.* 7:175–179.

Casjens, S., and R. Hendrix. 1988. Control mechanisms in dsDNA bacteriophage assembly. *In* The Bacteriophages, Vol. 1. R. Calender, editor. Plenum Publishing, New York. 15–91.

Casjens, S., and J. King. 1974. P22 morphogenesis. I. Catalytic scaffolding protein in capsid assembly. *J. Supramol. Struct.* 2:202–224.

Caspar, D. L. D., and A. Klug. 1962. Physical principles in the construction of regular viruses. *Cold Spring Harb. Symp. Quant. Biol.* 27:1–32.

Cepko, C. L., and P. A. Sharp. 1982. Assembly of adenovirus major capsid protein is mediated by a non-virion protein. *Cell.* 31:407–415.

Conway, J. F., R. L. Duda, R. W. Hendrix, and A. C. Steven. 1995. Proteolytic and conformational control of virus capsid maturation: the bacteriophage HK97 system. *J. Mol. Biol.* 253:86–99.

Crowther, R. A. 1971. Procedures for three-dimensional reconstruction of spherical viruses by Fourier synthesis from electron micrographs. *Philos. Trans. R. Soc. Lond. B.* 261:221–230.

Crowther, R. A., N. A. Kiselev, B. Botcher, J. A. Berriman, G. P. Borisova, V. Ose, and P. Pumpens. 1994. Three-dimensional structure of hepatitis B virus core particles determined by electron cryomicroscopy. *Cell.* 77:943–950.

Crowther, R. A., D. J. DeRosier, and A. Klug. 1970. The reconstruction of a three-dimensional structure from projections and its application to electron microscopy. *Proc. R. Soc. Lond.* 317:319–340.

D'Halluin, J.-C. M., G. R. Martin, G. Torpier, and P. Boulanger. 1978. Adenovirus type 2 assembly analysed by reversible cross-linking of labile intermediates. *J. Virol.* 26:357–363.

Dokland, T., B. H. Lindquist, and S. D. Fuller. 1992. Image reconstruction from cryo-electron micrographs reveals the morphopoetic mechanism in the P2–P4 bacteriophage system. *EMBO J.* 11:839–846.

Dokland, T., R. McKennal, L. L. Ilagl, B. R. Bowmanl, N. L. Incardona, B. A. Fane, and M. G. Rossmann. 1997. Structure of a viral procapsid with molecular scaffolding. *Nature.* 389:308–313.

Dokland, T., and H. Murialdo. 1993. Structural transitions during maturation of bacteriophage lambda capsids. *J. Mol. Biol.* 233:682–694.

Dubochet, J., M. Adrian, J. J. Chang, J. C. Homo, J. Lepault, A. W. McDowall, and P. Schultz. 1988. Cryo-electron microscopy of vitrified specimens. *Q. Rev. Biophys.* 21:129–228.

Earnshaw, W., and J. King. 1978. Structure of phage P22 coat protein aggregates formed in the absence of the scaffolding protein. *J. Mol. Biol.* 126:721–747.

Edvardsson, B., E. Everitt, H. Jornvall, L. Prage, and L. Philipson. 1976. Intermediates in adenovirus assembly. *J. Virol.* 19:533–547.

Frank, J., A. Verschoor, and M. Boublik. 1981. Computer averaging of electron micrographs of 40S ribosomal subunits. *Science.* 214: 1353–1355.

Fukami, A., and K. Adachi. 1965. A new method of preparation of a self-perforated micro plastic grid and its application (I). *J. Electron. Microsc. (Tokyo).* 14:112–118.

Fuller, M. T., and J. King. 1981. Purification of the coat and scaffolding protein from procapsids of bacteriophages P22. *Virology.* 112:529–547.

Fuller, S. D. 1987. The $T = 4$ envelope of Sindbis virus is organized by interactions with a complementary $T = 3$ capsid. *Cell.* 48:923–934.

Greene, B., and J. King. 1994. Binding of scaffolding subunits within the P22 procapsid lattice. *Virology.* 205:188–197.

Greene, B., and J. King. 1996. Scaffolding mutants identifying domains required for P22 procapsid assembly and maturation. *Virology.* 225: 82–96.

Hirokawa, N. 1994. Microtubule organization and dynamics dependent on microtubule associated proteins. *Curr. Opin. Cell Biol.* 6:74–81.

Ilag, L., N. Olson, T. Dokland, C. Music, R. Cheng, Z. Bowen, R. McKenna, M. Rossman, T. Baker, and N. Incardona. 1995. DNA packaging intermediates of bacteriophage φX174. *Structure.* 3:353–363.

Johnson, J. E. 1996. Functional implications of protein-protein interactions in icosahedral viruses. *Proc. Natl. Acad. Sci. USA.* 93:27–33.

Katsura, I. 1983. Structure and inherent properties of the bacteriophage λ head shell. IV. Small-head mutants. *J. Mol. Biol.* 171:297–317.

Keen, J. H. 1990. Clathrin and associated assembly and disassembly proteins. *Annu. Rev. Biochem.* 59:415–438.

King, J., and S. Casjens. 1974. Catalytic head assembling protein in virus morphogenesis. *Nature.* 251:112–119.

King, J., E. V. Lenk, and D. Botstein. 1973. Mechanism of head assembly and DNA maturation in *Salmonella* phage P22. II. Morphogenetic pathway. *J. Mol. Biol.* 80:697–731.

Lawton, J. A., and B. V. V. Prasad. 1996. Automated software package for icosahedral virus reconstruction. *J. Struct. Biol.* 116:209–215.

Mandelkow, E., and E.-M. Mandelkow. 1995. Microtubules and microtubule-associated d proteins. *Curr. Opin. Cell Biol.* 7:72–81.

Marvik, O. J., T. Dokland, R. H. Nokling, E. Jacobsen, T. Larsen, and B. H. Lindqvist. 1995. The capsid size-determining protein Sid forms an external scaffold on phage P4 procapsids. *J. Mol. Biol.* 251:59–75.

Matusick-Kumar, L., W. Hurlburt, S. P. Weinheimer, W. W. Newcomb, J. C. Brown, and M. Gao. 1994. Phenotype of the herpes simplex virus type-1 protease substrate ICP35 mutant virus. *J. Virol.* 68:5384–5394.

McGough, A. 1998. F-actin-binding proteins. *Curr. Opin. Struct. Biol.* 8:166–176.

McGough, A., M. Way, and D. DeRosier. 1994. Determination of the alpha-actinin binding site on actin filaments by cryoelectron microscopy and image analysis. *J. Cell Biol.* 126(2):433–443.

Milligan, R. A., and P. F. Flicker. 1987. Structural relationships of actin, myosin, and tropomyosin revealed by cryo-electron microscopy. *J. Cell Biol.* 105:29–39.

Newcomb, W. W., F. L. Homa, D. R. Thomsen, F. P. Booy, B. L. Trus, A. C. Steven, J. V. Spencer, and J. C. Brown. 1996. Assembly of the herpes simplex virus capsid: characterization of intermediates observed during cell-free capsid formation. *J. Mol. Biol.* 263:432–446.

Parker, M., S. Casjens, and P. E. Prevelige, Jr. 1998. Functional domains of bacteriophage P22 scaffolding protein. *J. Mol. Biol.* 281:69–79.

Parker, M. H., W. F. Stafford, III, and P. E. Prevelige, Jr. 1997. Bacteriophage P22 scaffolding protein forms oligomers in solution. *J. Mol. Biol.* 268:655–665.

Prasad, B. V. V., P. E. Prevelige, E. Marietta, R. O. Chen, D. Thomas, J. King, and W. Chiu. 1993. Three-dimensional transformation of capsids associated with genome packaging in a bacterial virus. *J. Mol. Biol.* 231:65–74.

Prevelige, P. E., T. J. Dennis, and J. King. 1988. Scaffolding protein regulates the polymerization of P22 coat subunits into icosahedral shells in vitro. *J. Mol. Biol.* 202:743–757.

Prevelige, P. E., Jr., D. Thomas, A. L. Kelly, S. A. Towse, and G. J. Thomas, Jr. 1993a. Subunit conformational changes accompanying bacteriophage P22 capsid maturation. *Biochemistry.* 32:537–543.

Prevelige, P. E., D. Thomas, and J. King. 1993b. Nucleation and growth phases in the polymerization of coat and scaffolding subunits into icosahedral procapsid shells. *Biophys. J.* 64:824–835.

Radermacher, M. 1988. Three-dimensional reconstruction of single particles from random and nonrandom tilt series. *J. Electron. Microsc. Tech.* 9:359–394.

Ray, P., and H. Murialdo. 1975. The role of gene Nu3 in bacteriophage lambda head morphogenesis. *Virology.* 64:247–263.

Rixon, F. J. 1993. Structure and assembly of herpesviruses. *Semin. Virol.* 4:135–144.

Roeder, G. S., and P. D. Sadowski. 1977. Bacteriophage T7 morphogenesis: phage related particles in cells infected with wild-type and mutant T7 phage. *Virology.* 76:263–285.

Schrag, J. D., B. V. V. Prasad, F. J. Rixon, and W. Chiu. 1989. Three-dimensional structure of the HSV1 nucleocapsid. *Cell.* 56:651–660.

Stewart, P. L., S. D. Fuller, and R. M. Burnett. 1993. Difference imaging of adenovirus: bridging the resolution gap between x-ray crystallography and electron microscopy. *EMBO J.* 12:2589–2599.

Tatman, J. D., V. G. Preston, P. Nicholson, R. M. Elliott, and F. J. Rixon. 1994. Assembly of herpes simplex virus type 1 capsids using a panel of recombinant baculoviruses. *J. Gen. Virol.* 75:1101–1113.

Thomsen, D. R., L. L. Roof, and F. L. Homa. 1994. Assembly of herpes simplex virus (HSV) intermediate capsids in insect cells infected with recombinant Baculoviruses expressing HSV capsid proteins. *J. Virol.* 68:2442–2457.

Thuman-Commike, P. A., and W. Chiu. 1995. Automatic detection of spherical particles from spot-scan electron microscopy images. *J. Microsc. Soc. Am.* 1:191–201.

Thuman-Commike, P. A., and W. Chiu. 1996. PTOOL: a software package for the selection of particles from electron cryomicroscopy spot-scan images. *J. Struct. Biol.* 116:41–47.

Thuman-Commike, P. A., and W. Chiu. 1997. Improved common-line based icosahedral virus particle image orientation estimation algorithms. *Ultramicroscopy.* 68:231–256.

Thuman-Commike, P. A., B. Greene, J. Jakana, B. V. V. Prasad, J. King, P. E. Prevelige, Jr., and W. Chiu. 1996. Three-dimensional structure of scaffolding-containing phage P22 procapsids by electron cryomicroscopy. *J. Mol. Biol.* 260:85–98.

Thuman-Commike, P., B. Greene, J. A. Malinski, J. King, and W. Chiu. 1998. Role of the scaffolding protein in P22 procapsid size determination suggested by $T = 4$ and $T = 7$ procapsid structures. *Biophys. J.* 74:559–568.

Toyoshima, C. 1989. On the use of holey grids in electron crystallography. *Ultramicroscopy.* 30:439–444.

Trachtenberg, S., and D. DeRosier. 1987. Three-dimensional structure of the frozen, hydrated flagellar filament. The left-handed filament of *Salmonella typhimurium*. *J. Mol. Biol.* 195:581–601.

Trus, B. L., F. P. Booy, W. W. Newcomb, J. C. Brown, F. L. Homa, D. R. Thomsen, and A. C. Steven. 1996. The herpes simplex virus procapsid: structure, conformational changes upon maturation, and roles of the triplex proteins V19c and VP23 in assembly. *J. Mol. Biol.* 263:447–462.

Tuma, R., M. Parker, P. Weigele, L. Sampson, Y. Sun, N. Krishna, S. Casjens, G. Thomas, Jr., and P. Prevelige, Jr. 1998. A helical coat protein recognition domain of the bacteriophage P22 scaffolding protein. *J. Mol. Biol.* 281:81–94.

van Heel, M. 1987. Similarity measures between images. *Ultramicroscopy.* 21:95–100.

Venien-Bryan, C., and S. D. Fuller. 1994. The organization of the spike complex of Semliki forest virus. *J. Mol. Biol.* 236:572–583.

Zhou, Z. H., W. Chiu, K. Haskell, H. J. Spears, J. Jakana, F. J. Rixon, and L. R. Scott. 1998a. Refinement of herpesvirus B-capsid structure on parallel supercomputers. *Biophys. J.* 74:576–588.

Zhou, Z. H., S. Hardt, B. Wang, M. B. Sherman, J. Jakana, and W. Chiu. 1996. CTF determination of images of ice-embedded single particles using a graphics interface. *J. Struct. Biol.* 116:216–222.

Zhou, Z., S. Macnab, J. Jakana, L. Scott, W. Chiu, and F. Rixon. 1998b. Identification of the sites of interaction between the scaffold and outer shell in herpes simplex virus-1 capsids by difference electron imaging. *Proc. Natl. Acad. Sci. USA.* 95:2778–2783.

Zhou, Z. H., B. V. V. Prasad, J. Jakana, F. Rixon, and W. Chiu. 1994. Protein subunit structures in the herpes simplex virus A-capsid determined from 400 kV spot-scan electron cryomicroscopy. *J. Mol. Biol.* 242:458–469.